Article

Not peer-reviewed version

Three-Temperature Boundary Element Modeling of Ultrasound Wave Propagation in Anisotropic Viscoelastic Porous Media

Mohamed Abdelsabour Fahmy * , Mohammed O. Alsulami , Ahmed E. Abouelregal

Posted Date: 25 April 2023

doi: 10.20944/preprints202304.0908.v1

Keywords: Boundary element model; Ultrasonic wave propagation; Three-temperature; Anisotropic viscoelastic porous media

Article

Three-Temperature Boundary Element Modeling of Ultrasound Wave Propagation in Anisotropic Viscoelastic Porous Media

Mohamed Abdelsabour Fahmy [1,2,*], Mohammed O. Alsulami [3] and Ahmed E. Abouelregal [4,5]

[1] Adham University College, Umm Al-Qura University, Adham 28653, Makkah, Saudi Arabia; maselim@uqu.edu.sa
[2] Department of Mathematical Sciences, Faculty of Applied Sciences Umm Al-Qura University, Makkah 24381, Saudi Arabia; s44285534@st.uqu.edu.sa
[3] Department of Mathematics, College of Science and Arts, Jouf University, Al-Qurayyat 72388, Saudi Arabia; ahabogal@ju.edu.sa
[4] Department of Mathematics, Faculty of Science, Mansoura University, Mansoura 35516, Egypt
* Correspondence: maselim@uqu.edu.sa; Tel.: 00966537930306

Abstract: The main goal of this work is to develop a novel boundary element method (BEM) model for analyzing ultrasonic wave propagation in three-temperature anisotropic viscoelastic porous media. Because of strong nonlinearity of ultrasonic wave propagation in three-temperature porous media problems, the analytical or numerical solutions to the problems under consideration are always challenging, necessitating the development of new computational techniques. As a result, we use a new BEM model to solve such problems. A time stepping procedure based on the linear multistep method is obtained after solving the discretized boundary integral equation with the quadrature rule. The calculation of a double integral is required to obtain fundamental solutions, but this increases the total BEM computation time. Our proposed BEM technique is used to solve the current problem and improve the formulation efficiency. The numerical results are graphed to demonstrate the effects of viscosity and anisotropy on the nonlinear ultrasonic stress waves in three-temperature porous media. The validity, accuracy, and efficiency in the proposed methodology were demonstrated by comparing obtained results to the corresponding solution obtained from finite difference method (FDM).

Keywords: boundary element model; ultrasonic wave propagation; three-temperature; anisotropic viscoelastic porous media

MSC: 35Qxx, 65Zxx

1. Introduction

In recent years, many engineering studies have drawn researchers' attention to investigate the mechanical behaviour of viscoelastic porous materials [1–6] due to the positive results obtained in applied science, engineering, and technological applications such as biology, biophysics, biomechanics, geotechnical engineering, reservoir geomechanics, mining and petroleum engineering, geothermal engineering, thermal insulation, and lightweight structural design. Some researchers have investigated the effects of magnetic field [7], initial stress [8], rotation and gravity [9] on the generalized thermo-viscoelastic diffusion medium. Also, the effects of initial stress and temperature-dependent on the thermo-microstretch elastic solid have been investigated with dual-phase-lag model [10]. Xu et al. [11] studied the effects of viscoelastic dampers with high energy dissipation based on an acrylate rubber matrix. Because analytical solutions to the current situation are extremely difficult to achieve, numerical methods have emerged as the primary tool for resolving these problems such as Pei et al. [12], Ooi et al. [13], Zhou et al. [14], Ng et al. [15], Majchrzak and Turchan [16], Bottauscio et al. [17], Deng and Liu [18] and Partridge and Wrobel [19]. The concept of

Preprints (www.preprints.org) | NOT PEER-REVIEWED | Posted: 25 April 2023 doi:10.20944/preprints202304.0908.v1

treating biological tissue as a porous medium has been deemed more acceptable for incorporating blood flow through arteries implanted in the tissue. One of the computational strategies used to solve the bioheat transfer problems of biological tissues [20–22] is the boundary element method (BEM) [23–31]. For physical and technological problems, Laplace-domain fundamental solutions are generally easier to get than time-domain fundamental solutions [32,33]. As a result, because it requires the Laplace-domain fundamental solutions of the problem's governing equations, the CQBEM is highly useful for problems that did not have time-domain fundamental solutions. As a result, CQBEM broadens the spectrum of engineering problems that can be tackled using traditional time-domain BEM.

The primary goal of this paper is to present a new boundary element model for explaining thermomechanical interactions in three-temperature anisotropic viscoelastic porous media. The uncoupled governing equations are solved independently, where the bioheat equation is solved first using the GBEM based on LRBFCM to obtain the temperature distribution, and then the mechanical equation was solved using the CQBEM to obtain the displacements and stresses. The resulting linear systems have been solved by communication-avoiding Arnoldi (CA-Arnoldi) preconditioner which reduces the number of iterations and the total CPU time. The numerical results demonstrate the validity, efficiency and accuracy of the proposed model

2. Formulation of the Problem

In the Cartesian system (x, y, z), we consider a region $\Omega = \left\{0 < x < \underline{\alpha}, , 0 < y < \underline{\beta}, 0 < z < \underline{\gamma},\right\}$ with a boundary Γ occupied by an anisotropic viscoelastic porous media as shown in Figure 1.

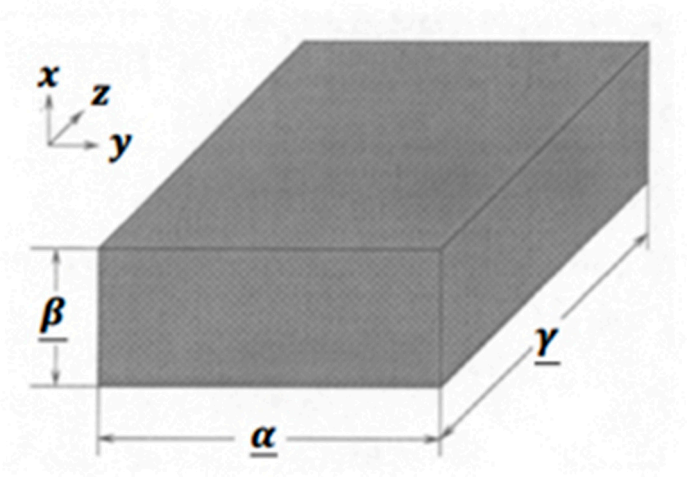

Figure 1. Computational domain of the current problem.

According to Biot's model [34] and Darcy's law [35], the thermo-poroelastic governing equations can be expressed as

$$(\nabla^T \sigma)^T + \mathbf{F} = \rho \ddot{\mathbf{u}} + \phi \rho_f \left(\ddot{\mathbf{u}}_f - \ddot{\mathbf{u}}\right) \tag{1}$$

$$\dot{\zeta} + \nabla^T \mathbf{q} = 0) \tag{2}$$

$$\sigma = \left(C_{ajlg}(\tau)\, \chi\, \mathrm{tr}\, \epsilon - A\bar{p}\right)\mathbf{I} - \mathfrak{B}\, \theta \tag{3}$$

$$\epsilon = \frac{1}{2}(\nabla \mathbf{u}^T + (\nabla \mathbf{u}^T)^T) \tag{4}$$

$$\zeta = A\, \mathrm{tr}\, \epsilon + \frac{\phi^2}{R}\bar{p} \tag{5}$$

Preprints (www.preprints.org) | NOT PEER-REVIEWED | Posted: 25 April 2023 doi:10.20944/preprints202304.0908.v1

$$\mathbf{q} = -K\left(\nabla \bar{p} + \rho_f \ddot{\mathbf{u}} + \frac{\rho_e + \phi\rho_f}{\phi}\left(\ddot{\mathbf{u}}_f - \ddot{\mathbf{u}}\right)\right) \tag{6}$$

On the basis of Bonnet [36], the governing equations can be written as follows [37]

$$\left.\begin{array}{l} \hat{B}_{\tilde{x}}\hat{\mathbf{u}}^g(\tilde{\mathbf{x}}) = 0 \ \text{ for } \tilde{x} \in \Omega \\ \hat{\mathbf{u}}^g(\mathbf{x}) = \hat{g}_D \ \text{ for } x \in \Gamma_D \\ \hat{\mathbf{t}}^g(\mathbf{x}) = \hat{g}_N \ \text{ for } x \in \Gamma_N \end{array}\right\} \tag{7}$$

in which where the operator $\hat{B}_{\tilde{\mathrm{x}}}$ and the tractions $\hat{t}^g$ are defined as

$$\hat{B}_{\tilde{\mathrm{x}}} = \begin{bmatrix} B^e_{\tilde{\mathrm{x}}} + s^2(\rho - \beta\rho_f)I & (\alpha-\beta)\nabla_{\tilde{\mathrm{x}}} & -\mathfrak{B}\nabla_{\tilde{\mathrm{x}}} \\ s(\alpha-\beta)\nabla^T_{\tilde{\mathrm{x}}} & -\dfrac{\beta}{s\rho_f}\Delta_{\tilde{\mathrm{x}}} + \dfrac{s\phi^2}{R} & 0 \end{bmatrix},$$

$$\hat{\mathbf{t}}^g(x) = \begin{bmatrix} T^e_{\mathrm{x}} & -\alpha\mathbf{n}_{\mathbf{x}} & 0 \\ s\beta\mathbf{n}^T_{\mathbf{x}} & \dfrac{\beta}{s\rho_f}\mathbf{n}^T_{\mathbf{x}}\nabla_{\mathrm{x}} & 0 \end{bmatrix}\begin{bmatrix} \hat{\mathbf{u}}(\mathbf{x}) \\ \hat{p}(\mathbf{x}) \\ \theta(\mathbf{x}) \end{bmatrix}, \qquad \beta = \frac{\phi^2 sK\rho_f}{\phi^2 + sK(\rho_e + \phi\rho_f)} \tag{8}$$

According to Fahmy [30], the thermomechanical interactions can be found by treating the soft tissue as a thermoporoelastic medium and implementing BEM for solving the governing equations (1) and (7).

The three-temperature radiative diffusion equations are as follows

$$C_{ve}\frac{\partial\theta_e(\mathrm{r},\tau)}{\partial\tau} - \frac{1}{\rho}\nabla[\mathbb{K}_e\,\nabla\theta_e(\mathrm{r},\tau)] = -\,\mathbb{W}_{ei}\,(\theta_e - \theta_i) - \mathbb{W}_{er}\,(\theta_e - \theta_r) \tag{9a}$$

$$C_{vi}\frac{\partial\theta_i(\mathrm{r},\tau)}{\partial\tau} - \frac{1}{\rho}\nabla[\mathbb{K}_i\,\nabla\theta_i(\mathrm{r},\tau)] = \mathbb{W}_{ei}\,(\theta_e - \theta_i) \tag{9b}$$

$$C_{vr}\frac{\partial\theta_r(\mathrm{r},\tau)}{\partial\tau} - \frac{1}{\rho}\nabla[\mathbb{K}_r\,\nabla\theta_r(\mathrm{r},\tau)] = \mathbb{W}_{er}\,(\theta_e - \theta_r) \tag{9c}$$

in which $C_{v\alpha} = \begin{cases} C_{v\alpha} = C_e & \alpha = e \\ C_{v\alpha} = C_i & \alpha = i \\ C_{v\alpha} = C_r T_r^3 & \alpha = r \end{cases}$ and $\mathbb{K}_\alpha = \begin{cases} \mathbb{A}_e\,T_e^{5/2} & \alpha = e \\ \mathbb{A}_i\,T_i^{5/2} & \alpha = i \\ \mathbb{A}_r\,T_r^{3+\mathbb{B}} & \alpha = r \end{cases}$

where e, i and r denote electron, ion, and phonon, respectively.

3. Boundary Element Implementation for the Temperature Field

The two-dimensions (2D) three-temperature (3T) radiation diffusion equations (9a) – (9c) can be written as

$$\nabla[\mathbb{K}_\alpha\,\nabla\theta_\alpha(\mathrm{r},\tau)] + \overline{\mathbb{W}}(\mathrm{r},\tau) = c_\alpha\rho\delta_1\frac{\partial\theta_\alpha(\mathrm{r},\tau)}{\partial\tau} + Q(\mathrm{r},\tau) \tag{10}$$

In which $Q(\mathrm{r},\tau) = \frac{1-R}{\mathbf{x}_0}e^{\left(-\frac{\mathrm{r}_\alpha}{\mathrm{r}_0}\right)J(\tau)}, J(\tau) = \frac{J_0\,\tau}{\tau_1^2}e^{-\frac{\tau}{\tau_1}}, a = 1,2,3.$

where

$$\overline{\mathbb{W}}(r,\tau) = \begin{cases} -\rho\,\mathbb{W}_{ei}\,(\theta_e - \theta_i) - \rho\,\mathbb{W}_{er}\,(\theta_e - \theta_r), \alpha = e, \delta_1 = 1 \\ \rho\,\mathbb{W}_{ei}\,(\theta_e - \theta_i), \qquad \alpha = i,\ \delta_1 = 1 \\ \rho\,\mathbb{W}_{er}\,(\theta_e - \theta_r), \qquad \alpha = r, \delta_1 = T_p^3 \end{cases}$$

The total energy per unit mass is as follows

$$P = P_e + P_i + P_r, P_e = c_e\theta_e, P_i = c_i\theta_i, P_r = \frac{1}{4}c_r\theta_r^4 \tag{11}$$

The conditions under consideration can be summarized as follows:

$$\theta_\alpha(x,y,0) = \theta^0_\alpha(x,y) = g_1(x,\tau) \tag{12}$$

Preprints (www.preprints.org) | NOT PEER-REVIEWED | Posted: 25 April 2023 doi:10.20944/preprints202304.0908.v1

$$\mathbb{K}_\alpha \frac{\partial \theta_\alpha}{\partial n}\Big|_{\Gamma_1} = 0, \alpha = e, i, \theta_p\big|_{\Gamma_1} = g_2(x,\tau) \tag{13}$$

$$\mathbb{K}_\alpha \frac{\partial \theta_\alpha}{\partial n}\Big|_{\Gamma_2} = 0, \alpha = e, i, r \tag{14}$$

Using the fundamental solution to the following differential equation

$$D\nabla^2\theta_\alpha + \frac{\partial \theta_\alpha^*}{\partial n} = -\delta(\mathrm{r} - p_i)\delta(\tau - \mathrm{r}), \qquad D = \frac{\mathbb{K}_\alpha}{\rho c} \tag{15}$$

The dual reciprocity boundary integral equation corresponding to (10) can be expressed as in Fahmy [17] as follows

$$C\theta_\alpha = \frac{D}{\mathbb{K}_\alpha}\int_O^\tau \int_S [\theta_\alpha q^* - \theta_\alpha^* q]\, dS\, d\tau + \frac{D}{\mathbb{K}_\alpha}\int_O^\tau \int_R b\,\theta_\alpha^*\, dR\, d\tau + \int_R \theta_\alpha^i \theta_\alpha^*\big|_{\tau=0}\, dR \tag{16}$$

which can be expressed as follows

$$C\theta_\alpha = \int_S [\theta_\alpha q^* - \theta_\alpha^* q]\, dS - \int_R \frac{\mathbb{K}_\alpha}{D}\frac{\partial \theta_\alpha^*}{\partial \tau}\theta_\alpha\, dR \tag{17}$$

We assume that the temperature derivative in (17) is approximated as

$$\frac{\partial \theta_\alpha}{\partial \tau} \cong \sum_{j=1}^{N} f^j(r)^j a^j(\tau) \tag{18}$$

Now, we consider

$$\nabla^2 \hat{\theta}_\alpha^j = f^j \tag{19}$$

Thus, from Equation (17), we obtain

$$C\,\theta = \int_S [\theta_\alpha q^* - \theta_\alpha^* q]\, dS + \sum_{j=1}^{N} a^j(\tau) D^{-1}\left(C\hat{\theta}_\alpha^j - \int_S [\theta_\alpha^j q^* - \hat{q}^j \theta_\alpha^*]\, dS\right) \tag{20}$$

where

$$\hat{q}^j = -\mathbb{K}_\alpha \frac{\partial \hat{\theta}_\alpha^j}{\partial n} \tag{21}$$

and

$$a^j(\tau) = \sum_{i=1}^{N} f_{ji}^{-1} \frac{\partial \theta(r_i,\tau)}{\partial \tau} \tag{22}$$

where f_{ji}^{-1} are defined as

$$\{F\}_{ji} = f^j(r_i) \tag{23}$$

By using equations (20) and (22), we get

$$C\,\dot{\theta}_\alpha + H\,\theta_\alpha = G\,Q \tag{24}$$

where

$$C = -[H\,\hat{\theta}_\alpha - G\,\hat{Q}]F^{-1}D^{-1} \tag{25}$$

with

$$\{\hat{\theta}\}_{ij} = \hat{\theta}^j(x_i) \tag{26}$$

$$\{\hat{Q}\}_{ij} = \hat{q}^j(x_i) \tag{27}$$

Now, we introduce the following functions

$$\theta_\alpha = (1 - \boldsymbol{\theta})\,\theta_\alpha^m + \boldsymbol{\theta}\,\theta_\alpha^{m+1} \tag{28}$$

Preprints (www.preprints.org) | NOT PEER-REVIEWED | Posted: 25 April 2023 doi:10.20944/preprints202304.0908.v1

$$q = (1-\boldsymbol{\theta})q^m + \boldsymbol{\theta}\, q^{m+1} \tag{29}$$

where $0 \le \boldsymbol{\theta} = \frac{\tau-\tau^m}{\Delta\tau^m} \le 1,\ \Delta\tau^m = \tau^{m+1} - \tau^m$.

By differentiating (28), we get

$$\dot{\theta}_\alpha = \frac{d\theta_\alpha}{d\boldsymbol{\theta}}\frac{d\boldsymbol{\theta}}{d\tau} = \frac{\theta_\alpha^{m+1} - \theta_\alpha^m}{\Delta\tau^m} \tag{30}$$

Substitution of Equations (31) - (33) into Equation (27), yields

$$\left(\frac{C}{\Delta\tau^m} + \boldsymbol{\theta}H\right)\theta_\alpha^{m+1} - \boldsymbol{\theta}GQ^{m+1} = \left(\frac{C}{\Delta\tau^m} - (1-\boldsymbol{\theta})H\right)\theta_\alpha^m + (1-\boldsymbol{\theta})GQ^m \tag{31}$$

which can be written as

$$\mathbb{a}\mathrm{X} = \mathbb{b} \tag{32}$$

To solve the resulting linear algebraic systems, the symmetric successive over-relaxation (SSOR) method without matrix inversion [38] was efficiently implemented.

4. Boundary Element Implementation for the Poroelastic Fields

The representation formula for problem (7) is as follows:

$$\hat{\mathbf{u}}^g(\tilde{\mathbf{x}}) = \left(\hat{V}\hat{t}^g\right)_\Omega(\tilde{\mathbf{x}}) - \left(\hat{K}\hat{\mathbf{u}}^g\right)_\Omega(\tilde{\mathbf{x}}) \text{ for } \tilde{\mathbf{x}} \in \boldsymbol{\Omega} \tag{33}$$

where the integral operators are

$$\left(\hat{V}\hat{\mathbf{t}}^g\right)_\Omega(\tilde{\mathbf{x}}) = \int_\Gamma \hat{\mathbf{U}}^T(\mathbf{y}-\tilde{\mathbf{x}})\hat{t}^g(\mathbf{y})\, ds_\mathbf{y} \tag{34}$$

$$\left(\hat{K}\hat{\mathbf{u}}^g\right)_\Omega(\tilde{\mathbf{x}}) = \int_\Gamma \left(\hat{T}_\mathbf{y}\hat{\mathbf{U}}\right)^T(\mathbf{y}-\tilde{\mathbf{x}})\hat{\mathbf{u}}^g(\mathbf{y})\, ds_\mathbf{y} \tag{35}$$

In the Laplace domain, the fundamental solution and associated traction are denoted as [9]

$$\hat{\mathbf{U}}(\mathrm{r}) = \begin{bmatrix} \hat{\mathbf{U}}^s(\mathrm{r}) & \hat{\mathbf{U}}^f(\mathrm{r}) & 0 \\ \left(\hat{\mathbf{P}}^s\right)^T(\mathrm{r}) & \hat{P}^f(\mathrm{r}) & 0 \end{bmatrix},\ \hat{T}_y = \begin{bmatrix} T_\mathbf{y}^e & s\alpha\mathbf{n}_\mathbf{y} & 0 \\ -\beta\mathbf{n}_\mathbf{y}^T & \frac{\beta}{s\rho^f}\mathbf{n}_\mathbf{y}^T\nabla & 0 \end{bmatrix} \text{ with } \mathrm{r} := |\mathbf{y}-\mathbf{x}| \tag{36}$$

The fundamental solution can be expressed as [35]

$$\hat{\mathbf{U}}^s(\mathrm{r}) = \frac{1}{4\pi\mathrm{r}(\rho-\beta\rho^f)}\left[\mathbb{R}_1\frac{(k_4^2-k_2^2)}{(k_1^2-k_2^2)}e^{-k_1\mathrm{r}} - \mathbb{R}_2\frac{(k_4^2-k_1^2)}{(k_1^2-k_2^2)}e^{-k_2\mathrm{r}} + (Ik_3^2 - \mathbb{R}_3)e^{-k_3\mathrm{r}}\right] \tag{37}$$

where

$$\mathbb{R}_j = \frac{3\nabla_\mathbf{y}\mathrm{r}\nabla_\mathbf{y}^T\mathrm{r} - I}{\mathrm{r}^2} + k_j\frac{3\nabla_\mathbf{y}\mathrm{r}\nabla_\mathbf{y}^T\mathrm{r} - I}{\mathrm{r}} + k_j^2\nabla_\mathbf{y}\mathrm{r}\nabla_\mathbf{y}^T\mathrm{r} \tag{38}$$

Equation (37) can be expressed as

$$\hat{\mathbf{U}}^s(\mathrm{r}) = \frac{1}{4\pi\mu\mathrm{r}(\lambda+2\mu)}\left[(\lambda+\mu)\nabla_\mathbf{y}r\nabla_\mathbf{y}^T\mathrm{r} + I(\lambda+3\mu)\right] + O(\mathrm{r}^0) \tag{39}$$

The fundamental solution can be expressed as

$$\begin{aligned} \hat{\mathbf{U}}^s(\mathrm{r}) &= \hat{\mathbf{U}}_s^s(\mathrm{r}) + \hat{\mathbf{U}}_r^s(\mathrm{r}) \\ &= \frac{1}{\mu}\left[I\Delta_\mathbf{y} - \frac{\lambda+\mu}{\lambda+2\mu}\nabla_\mathbf{y}\nabla_\mathbf{y}^T\right]\Delta_\mathbf{y}\hat{\mathbf{x}}(\mathrm{r}) \\ &-\frac{1}{\mu}\left[\left(k_1^2+k_2^2\right)\Delta_y - k_1^2k_2^2\right)I - \left(k_1^2+k_2^2-k_4^2-\frac{k_1^2k_2^2}{k_3^2}\right)\nabla_\mathbf{y}\nabla_\mathbf{y}^T\Big]\hat{\mathbf{x}}(\mathrm{r}) \end{aligned} \tag{40}$$

in which

Preprints (www.preprints.org) | NOT PEER-REVIEWED | Posted: 25 April 2023 doi:10.20944/preprints202304.0908.v1

$$\hat{\mathbf{x}}(\mathrm{r}) = \frac{1}{4\pi r}\left[\frac{e^{-k_1\mathrm{r}}}{(k_2^2-k_1^2)(k_3^2-k_1^2)} + \frac{e^{-k_2\mathrm{r}}}{(k_2^2-k_1^2)(k_2^2-k_3^2)} + \frac{e^{-k_3\mathrm{r}}}{(k_1^2-k_3^2)(k_2^2-k_3^2)}\right]$$
$$= -\frac{1}{(k_1^2-k_2^2)(k_1^2-k_3^2)(k_3^2-k_2^2)} + O(\mathrm{r}^2) \tag{41}$$

Furthermore, the remaining components of the fundamental solution might be stated as

$$\hat{\mathbf{U}}^f(\mathrm{r}) = \frac{\rho^f(\alpha-\beta)\nabla_y \mathrm{r}}{4\pi r\beta(\lambda+2\mu)(k_1^2-k_2^2)}\left[\left(k_1+\frac{1}{\mathrm{r}}\right)e^{-k_1\mathrm{r}} - \left(k_2+\frac{1}{\mathrm{r}}\right)e^{-k_2\mathrm{r}}\right] = O(\mathrm{r}^0) \tag{42}$$

$$\hat{\mathbf{P}}^s(\mathrm{r}) = \frac{\hat{\mathbf{U}}^f(\mathrm{r})}{s} = O(\mathrm{r}^0) \tag{43}$$

$$\hat{P}^f(\mathrm{r}) = \frac{s\rho^f}{4\pi r\beta(k_1^2-k_2^2)}[(k_1^2-k_4^2)e^{-k_1 r} - (k_2^2-k_4^2)e^{-k_2 r}] = \frac{s\rho^f}{4\pi r\beta} + O(\mathrm{r}^0) \tag{44}$$

Now, we apply the following limiting $\tilde{\mathbf{x}} \in \Omega \to \mathbf{x} \in \Gamma$ to (34) to obtain

$$\lim_{\tilde{\mathbf{x}}\in\Omega\to\mathbf{x}\in\Gamma}\left(\hat{V}\hat{\mathbf{t}}^g\right)_\Omega(\tilde{\mathbf{x}}) = \left(\hat{V}\hat{\mathbf{x}}^g\right)(\mathbf{x}) \coloneqq \dot{\int_\Gamma}\hat{\mathbf{U}}^T(\mathbf{y}-\mathbf{x})\hat{\mathbf{t}}^g(\mathbf{y})ds_{\mathbf{y}} \tag{45}$$

In addition, we apply the following limiting method to (35) to obtain [39]

$$\lim_{\tilde{x}\in\Omega\to x\in\Gamma}\left(\hat{K}\hat{\mathbf{u}}^g\right)_\Omega(\tilde{\mathbf{x}}) = [-I(\mathbf{x}) + C(\mathbf{x})]\hat{\mathbf{u}}^g(\mathbf{x}) + \left(\hat{K}\hat{\mathbf{u}}^g\right)(\mathbf{x}) \tag{46}$$

in which

$$C(\mathbf{x}) = \lim_{\varepsilon\to 0}\dot{\int_{y\in\Omega:|y-x|=\varepsilon}}\left(\hat{T}_{\mathbf{y}}\hat{\mathbf{U}}\right)^T(\mathbf{y}-\mathbf{x})\,ds_{\mathbf{y}} \tag{47}$$

and

$$\left(\hat{K}\hat{\mathbf{u}}^g\right)(\mathbf{x}) = \lim_{\varepsilon\to 0}\dot{\int_{|y-x|\geq\varepsilon}}\left(\hat{T}_{\mathbf{y}}\hat{\mathbf{U}}\right)^T(\mathbf{y}-\mathbf{x})\,\hat{\mathbf{u}}^g(\mathbf{y})ds_{\mathbf{y}} \tag{48}$$

By using equations (45) - (48), the boundary integral equation in Laplace domain can be expressed as

$$C(\mathbf{x})\,\hat{\mathbf{u}}^g(\mathbf{x}) = \left(\hat{V}\hat{\mathbf{t}}^g\right)(\mathbf{x}) - \left(\hat{K}\hat{\mathbf{u}}^g\right)(\mathbf{x}) \tag{49}$$

The poroelastodynamic boundary integral equation can be expressed using the inverse Laplace transformation as

$$C(\mathbf{x})\mathbf{u}^g(\mathbf{x},t) = (V * \mathbf{t}^g)(\mathbf{x},t) - (K\mathbf{u}^g)(\mathbf{x},t) \tag{50}$$

The fundamental solution is as follows [37]

$$\left(\hat{T}_{\mathbf{y}}\hat{\mathbf{U}}\right)^T = \begin{bmatrix}\begin{bmatrix}\hat{T}_{\mathbf{y}}^e & s\alpha\mathbf{n}_{\mathbf{y}}\\ -\beta\mathbf{n}_{\mathbf{y}}^T & \frac{\beta}{s\rho_0^f}\mathbf{n}_{\mathbf{y}}^T\nabla_{\mathbf{y}}\end{bmatrix}\begin{bmatrix}\hat{\mathbf{U}}^s & \hat{\mathbf{U}}^f\\ \left(\hat{\mathbf{P}}^s\right)^T & \hat{P}^f\end{bmatrix}\end{bmatrix}^T = \begin{bmatrix}\hat{\mathbf{T}}^s & \hat{\mathbf{T}}^f\\ \left(\hat{\mathbf{Q}}^s\right)^T & \hat{Q}^f\end{bmatrix}^T \tag{51}$$

The Stokes theorem states that the differentiable vector field $\mathrm{a}(y),\ (y\in\Gamma)$ can be represented as

$$\dot{\int_\Gamma}(\nabla_{\mathbf{y}}\times\mathrm{a}, n_{\mathbf{y}})\,ds_{\mathbf{y}} = -\dot{\int_{\partial\Gamma}}(\mathrm{a},v)\,d\gamma_{\mathbf{y}} = -\dot{\int_\phi}(\mathrm{a},v)\,d\gamma_{\mathbf{y}} = 0 \tag{52}$$

where

$$\dot{\int_\Gamma}(n_{\mathbf{y}}\times\nabla_{\mathbf{y}},\mathrm{a})\,ds_{\mathbf{y}} = 0 \tag{53}$$

Preprints (www.preprints.org) | NOT PEER-REVIEWED | Posted: 25 April 2023 doi:10.20944/preprints202304.0908.v1

We can use (53) to obtain the following formula

$$\int_{\dot{\Gamma}} (M_{\mathbf{y}}\, \mathrm{a}\,)\, ds_{\mathbf{y}} = 0, \qquad M_{\mathbf{y}} = \left(\nabla_{\mathbf{y}} \nabla_{\mathbf{y}}^{T}\right)^{T} - \nabla_{\mathbf{y}} \nabla_{\mathbf{y}}^{T}, \qquad \mathrm{a} = vu \tag{54}$$

According to [40], we obtain

$$\int_{\dot{\Gamma}} (M_{\mathbf{y}}\, v)\, \mathbf{u} ds_{\mathbf{y}} = -\int_{\dot{\Gamma}} v(M_{\mathbf{y}}\ \mathbf{u})\, ds_{\mathbf{y}} \tag{55}$$

$$\int_{\dot{\Gamma}} (M_{\mathbf{y}}\, v)^{T}\, \mathbf{u} ds_{\mathbf{y}} = \int_{\dot{\Gamma}} v^{T}\, (M_{\mathbf{y}}\, \mathbf{u}) ds_{\mathbf{y}} \tag{56}$$

By using (40) and (51), we obtain

$$\left(\hat{\mathbf{T}}^{s}\right)^{T} = \left(T_{\mathbf{y}}^{e}\left(\hat{\mathbf{U}}_{sing}^{s} + \hat{\mathbf{U}}_{reg}^{s}\right)\right)^{T} + s\alpha \hat{P}^{s} \mathbf{n}_{\mathbf{y}}^{T} = \left(T_{\mathbf{y}}^{e}\ \hat{\mathbf{U}}_{sing}^{s}\right)^{T} + O(\mathrm{r}^{0}) \tag{57}$$

According to [37], we get

$$\left(\hat{\mathbf{T}}^{s}\right)^{T} = (\lambda + 2\mu) n_{\mathbf{y}} \nabla_{\mathbf{y}}^{T} \hat{\mathbf{U}}_{sing}^{s} - \mu\left(\boldsymbol{n}_{\mathbf{y}} \times \left(\nabla_{\mathbf{y}} \times \hat{\mathbf{U}}_{sing}^{s}\right)\right) + 2\mu M_{\mathbf{y}} \hat{\mathbf{U}}_{sing}^{s} + o(\mathrm{r}^{0}) \tag{58}$$

which can be expressed using (40) as

$$\left(\hat{\mathbf{T}}^{s}\right)^{T} = M_{\mathbf{y}} \Delta_{\mathbf{y}}^{2} \hat{X} + \mathbf{I}\left(\mathbf{n}^{T} \nabla_{\mathbf{y}}\right) \Delta_{\mathbf{y}}^{2} \hat{X} + 2\mu\left(M_{\mathbf{y}} \hat{\mathbf{U}}_{sing}^{s}\right)^{T} + o(\mathrm{r}^{0}) \tag{59}$$

Using (35) and (59), we obtain

$$\left(\hat{k}\hat{\mathbf{u}}\right)_{\Omega}^{s}(\tilde{\mathbf{x}}) = \int_{\dot{\Gamma}} \left[\left(M_{\mathbf{y}} \Delta_{\mathbf{y}}^{2} \hat{X}\right)\hat{\mathbf{u}} + \left(\mathbf{I}\left(\mathbf{n}^{T} \nabla_{\mathbf{y}}\right) \Delta_{\mathbf{y}}^{2} \hat{X}\right)\hat{\mathbf{u}} + 2\mu\left(M_{\mathbf{y}} \hat{\mathbf{U}}_{sing}^{s}\right)^{T} \hat{\mathbf{u}} + O(\mathrm{r}^{0})\hat{\mathbf{u}}\right] ds_{\mathbf{y}} \tag{60}$$

Based on [39], we get

$$\left(\hat{K}\hat{\mathbf{u}}\right)_{\Omega}^{s}(\tilde{\mathbf{x}}) = \int_{\dot{\Gamma}} \left[-\Delta_{\mathbf{y}}^{2} \hat{X}\left(M_{\mathbf{y}} \hat{\mathbf{u}}\right) + \left(\mathbf{I}\left(\mathbf{n}^{T} \nabla_{\mathbf{y}}\right) \Delta_{\mathbf{y}}^{2} \hat{x}\right)\hat{\mathbf{u}} + 2\mu \hat{U}_{s}^{s}\left(M_{\mathbf{y}} \hat{\mathbf{u}}\right) + O(\mathrm{r}^{0})\hat{\mathbf{u}}\right] ds_{\mathbf{y}} \tag{61}$$

The second term of the integral (61) can be expressed as

$$\left(\mathbf{n}^{T} \nabla_{\mathbf{y}}\right) \Delta_{\mathbf{y}}^{2} \hat{x}(\mathrm{r}) = \frac{\mathbf{n}^{T} \nabla_{\mathbf{y}^{r}}}{4\pi r^{2}} + O(\mathrm{r}^{0}) \tag{62}$$

where

$$C^{s}(\mathbf{x}) = I(\mathbf{x})\, c\,(\mathbf{x}) \quad \text{with} \quad c(\mathbf{x}) = \frac{\phi(\mathbf{x})}{4\pi} \tag{63}$$

Based on [37], the following limit may be rewritten as

$$\lim_{\Omega \ni \tilde{x} \to x \in \Gamma} \left(\hat{K}\hat{\mathbf{u}}\right)_{\Omega}^{s}(\tilde{\mathbf{x}}) = -I(\mathbf{x})[-1 + c(\mathbf{x})]\hat{\mathbf{u}}(\mathbf{x}) + \left(\hat{K}\hat{\mathbf{u}}\right)^{s}(\mathbf{x}) \tag{64}$$

By augmenting $\hat{U}_{s}^{s}$ to $\hat{U}^{s}$ and employing (56) we can write (61) as

$$\left(\hat{K}\hat{\mathbf{u}}\right)_{\Omega}^{s}(\tilde{\mathbf{x}}) = \int_{\dot{\Gamma}} -\Delta_{\mathbf{y}}^{2}\hat{\mathbf{x}}\left(M_{\mathbf{y}} \hat{\mathbf{u}}\right) + \left(\mathbf{I}\left(\mathbf{n}^{T} \nabla_{\mathbf{y}}\right) \Delta_{\mathbf{y}}^{2}\hat{\mathbf{x}}\right)\hat{\mathbf{u}} + 2\mu \hat{U}^{s}\left(M_{\mathbf{y}} \hat{\mathbf{u}}\right) + O(\mathrm{r}^{0})\hat{\mathbf{u}}\, ds_{\mathbf{y}} \tag{65}$$

By dividing the time interval $[0, T]$, we obtain the following integral

$$(f * g)(\tau) = \int_{0}^{t} f(\tau - t) g(t)\, dt \ \text{ for } \ \tau \in [0\,, T] \tag{66}$$

In which

$$(f * g)(\tau_{n}) \approx \sum_{k=0}^{n} \omega_{n-k}^{\Delta\tau}\left(\hat{f}\right) g(\tau_{k}) \tag{67}$$

According to Lubich formula [41,42], the integration weights ω_{n} can be determined as

Preprints (www.preprints.org) | NOT PEER-REVIEWED | Posted: 25 April 2023 doi:10.20944/preprints202304.0908.v1

$$\omega_n^{\Delta\tau}(\hat{f}) \coloneqq \frac{1}{2\pi i}\int_{|z|=R} \hat{f}\left(\frac{\gamma(z)}{\Delta\tau}\right) z^{-(n+1)}dz \tag{68}$$

Using $z = Re^{-i\varphi}$, the integral equation (68) may be approximated as

$$\omega_n^{\Delta\tau}(\hat{f}) \approx \frac{R^{-1}}{L+1}\sum_{\ell=o}^{L} \hat{f}\,(s_\ell)\zeta^{\,\ell n} \quad \text{with } \zeta = e^{\frac{2\pi i}{L+1}} \text{ and } s_\ell = \frac{\gamma\left(R\zeta^{-\ell}\right)}{\Delta\tau} \tag{69}$$

By plugging Equation (69) into Equation (67), we get

$$(f*g)(\tau_n) \approx \sum_{k=0}^{N} \frac{R^{-(n-k)}}{N+1}\sum_{\ell=0}^{N} \hat{f}\,(s_\ell)\zeta^{\ell(n-k)} g(\tau_k) \approx \frac{R^{-n}}{N+1}\sum_{\ell=0}^{N} \hat{f}\,(s_\ell)\hat{g}(s_\ell)\zeta^{\ell n} \tag{70}$$

with

$$\hat{g}(s_\ell) = \sum_{k=0}^{N} R^k\, g(\tau_k)\zeta^{-\ell k}. \tag{71}$$

Based on [39], we get

$$C(\mathbf{x})\mathbf{u}^g(\mathbf{x},\tau) = (v * \mathbf{t}^g)(\mathbf{x},\tau) - (k * \mathbf{u}^g)(\mathbf{x},\tau) \tag{72}$$

that can be expressed in Laplace domain as follows

$$C(\mathbf{x})\hat{\mathbf{u}}^g(\mathbf{x},s_\ell) = (\hat{v}\hat{\mathbf{t}}^g)(\mathbf{x},s_\ell) - \left(\hat{k}\hat{\mathbf{u}}^g\right)(\mathbf{x},s_\ell), \tag{73}$$

The discretization of the boundary $\Gamma = \partial\Omega$ into N_e boundary elements $\bar{\tau}_e$ leads to

$$\Gamma \approx \Gamma_h = \bigcup_{e=1}^{N_e} \bar{\tau}_e \tag{74}$$

Now, we use $\mathbb{i}$ continuous functions $\varphi_i^\alpha[k]$ and $\mathbb{j}$ discontinuous functions $\psi_j^\beta[k]$ to define the following subspaces

$$S_h[k]\left(\Gamma_{N,h}\right) \coloneqq span\{\varphi_i^\alpha[k]\}_{i=1}^{\mathbb{i}}, \qquad \alpha \geq 1 \tag{75}$$

$$S_h[k]\left(\Gamma_{D,h}\right) \coloneqq span\left\{\psi_j^\beta[k]\right\}_{j=1}^{\mathbb{j}}, \qquad \beta \geq 0 \tag{76}$$

By using (75) and (76), the unknown datum can be approximated as follows

$$\hat{\mathbf{u}}^g[k](\mathbf{x}) \approx \hat{\mathbf{u}}_h^g[k](\mathbf{x}) = \sum_{i=1}^{I} \hat{\mathbf{u}}_{h,i}^g[k]\varphi_i^\alpha[k](\mathbf{x}) \in S_h[k]\left(\Gamma_{N,h}\right), \tag{77}$$

$$\hat{\mathbf{t}}^g[k](\mathbf{x}) \approx \hat{\mathbf{t}}_h^g[k](\mathbf{x}) = \sum_{j=1}^{J} \hat{\mathbf{t}}_{h,j}^g[k]\psi_j^\beta[k](\mathbf{x}) \in S_h[k]\left(\Gamma_{D,h}\right), \tag{78}$$

Thus, we obtain

$$\begin{bmatrix} \hat{V}_{DD} & -\hat{K}_{DN} \\ \hat{V}_{ND} & -\left(C+\hat{K}_{NN}\right) \end{bmatrix}_\ell \begin{bmatrix} \hat{\mathbf{t}}_{D,h}^g \\ \hat{\mathbf{u}}_{N,h}^g \end{bmatrix}_\ell = \begin{bmatrix} -\hat{V}_{DN} & \left(C+\hat{K}_{DD}\right) \\ -\hat{V}_{NN} & \hat{K}_{ND} \end{bmatrix}_\ell \begin{bmatrix} \hat{g}_{N,h}^g \\ \hat{g}_{D,h}^g \end{bmatrix}_\ell \quad \ell = 0\ldots N \tag{79}$$

where

$$\hat{S}_{NN} \coloneqq \hat{V}_{ND}\hat{V}_{DD}^{-1}\hat{K}_{DN} - \left(C+\hat{K}_{NN}\right) \tag{80}$$

5. Numerical Results and Discussion

In the context of analyzing the BEM model results of solving ultrasonic wave propagation problems in three-temperature anisotropic viscoelastic porous media. As shown in Figure 2, the BEM discretization was carried out with 42 boundary elements and 68 internal points.

Preprints (www.preprints.org) | NOT PEER-REVIEWED | Posted: 25 April 2023 doi:10.20944/preprints202304.0908.v1

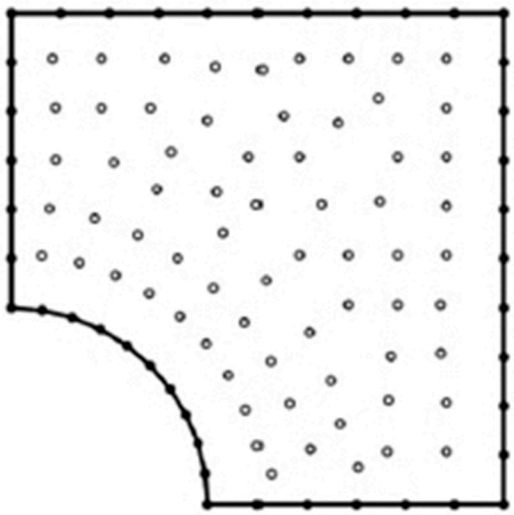

Figure 2. BEM model of the current problem.

To demonstrate the numerical results obtained by the proposed technique, the following physical parameters were used:

The elasticity tensor

$$C_{ablg} = \begin{bmatrix} C_{11} & C_{12} & C_{13} & 0 & 0 & 0 \\ C_{12} & C_{11} & C_{13} & 0 & 0 & 0 \\ C_{13} & C_{13} & C_{33} & 0 & 0 & 0 \\ 0 & 0 & 0 & C_{44} & 0 & 0 \\ 0 & 0 & 0 & 0 & C_{44} & 0 \\ 0 & 0 & 0 & 0 & 0 & C_{66} \end{bmatrix} \tag{81}$$

$$C_{11} = \frac{E^2 v_0^2 - E E_0}{(1+v)(2E v_0^2 + E_0(v-1))}, C_{12} = -\frac{E^2 v_0^2 + E E_0 v}{(1+v)(2E v_0^2 + E_0(v-1))}$$

$$C_{13} = -\frac{E E_0 v}{2E v_0^2 + E_0(v-1)}, C_{33} = -\frac{E_0^2 (v-1)}{2E v_0^2 + E_0(v-1)}$$

$$C_{44} = \mu_0, \; C_{66} = \frac{1}{2}(C_{11} - C_{12})$$

For anisotropic viscoelastic porous media, we considered the following physical parameters [43]

$$v = 0.95, v_0 = 0.49, \mu_0 = 20.98 \text{ GPa}, E = 22 \text{ kPa}, E_0 = 447 \text{ kPa}$$

and therefore

$$k_1 = 1243 \text{ kPa}, k_2 = 442 \text{ kPa}$$

and

$$\rho_s = 1600 \; kg/m^3, \; \rho_f = 1113 \; kg/m^3, \; p = 25 \; MPa, \; \phi = 0.15 \text{ and } Q/R = 0.65.$$

Figures 3, 4 and 5 show the distributions of the nonlinear thermal stress σ_{11}, σ_{12}, and σ_{22} waves along x_1-axis for electron, ion, phonon and total 3T with and without viscosity effect. Figure 3 shows the distribution of the nonlinear thermal stress σ_{11} waves for electron ($\theta = \theta_e$), ion ($\theta = \theta_i$), phonon ($\theta = \theta_r$), and total 3T ($\theta = \theta_e + \theta_i + \theta_r$) with and without viscosity effect. Figure 4 shows the distribution of the nonlinear thermal stress σ_{12} waves for electron ($\theta = \theta_e$), ion ($\theta = \theta_i$), phonon ($\theta = \theta_r$), and total ($\theta = \theta_e + \theta_i + \theta_r$) with and without viscosity effect. Figure 5 shows the distribution of the nonlinear thermal stress σ_{22} waves for electron ($\theta = \theta_e$), ion ($\theta = \theta_i$), phonon ($\theta = \theta_r$), and total ($\theta = \theta_e + \theta_i + \theta_r$) with and without viscosity effect.

Preprints (www.preprints.org) | NOT PEER-REVIEWED | Posted: 25 April 2023 doi:10.20944/preprints202304.0908.v1

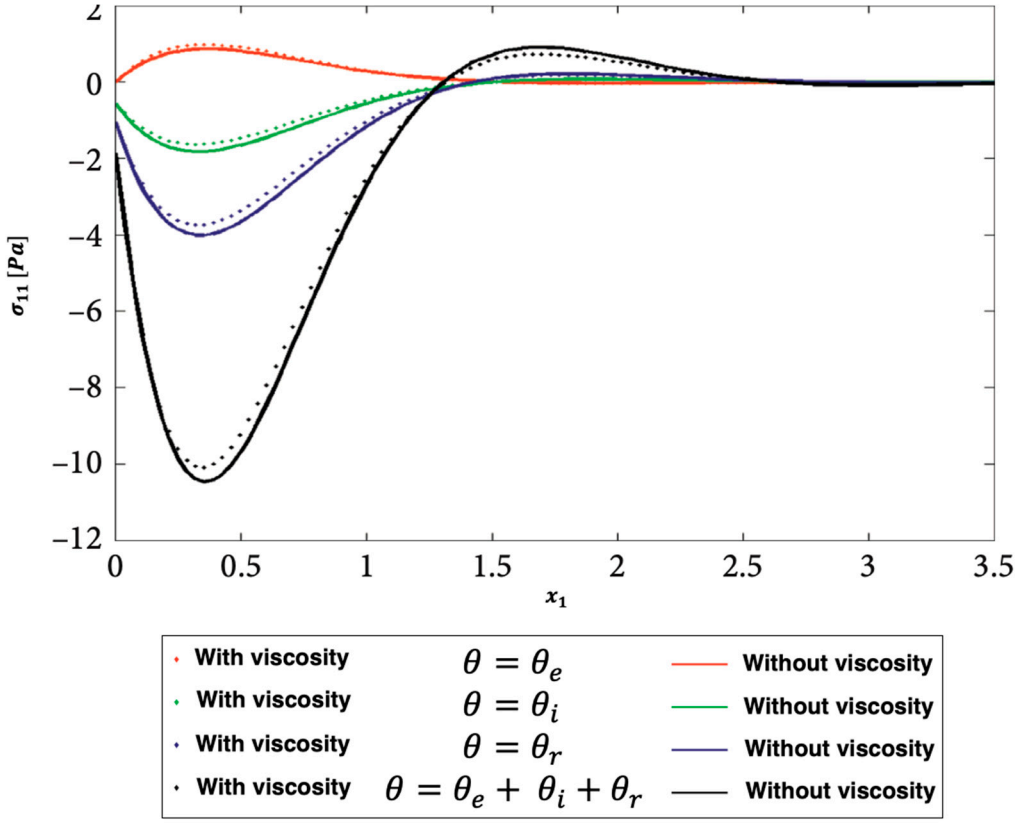

Figure 3. Propagation of the nonlinear thermal stress σ_{11} waves along x_1-axis for electron, ion, phonon and total 3T with and without viscosity effect.

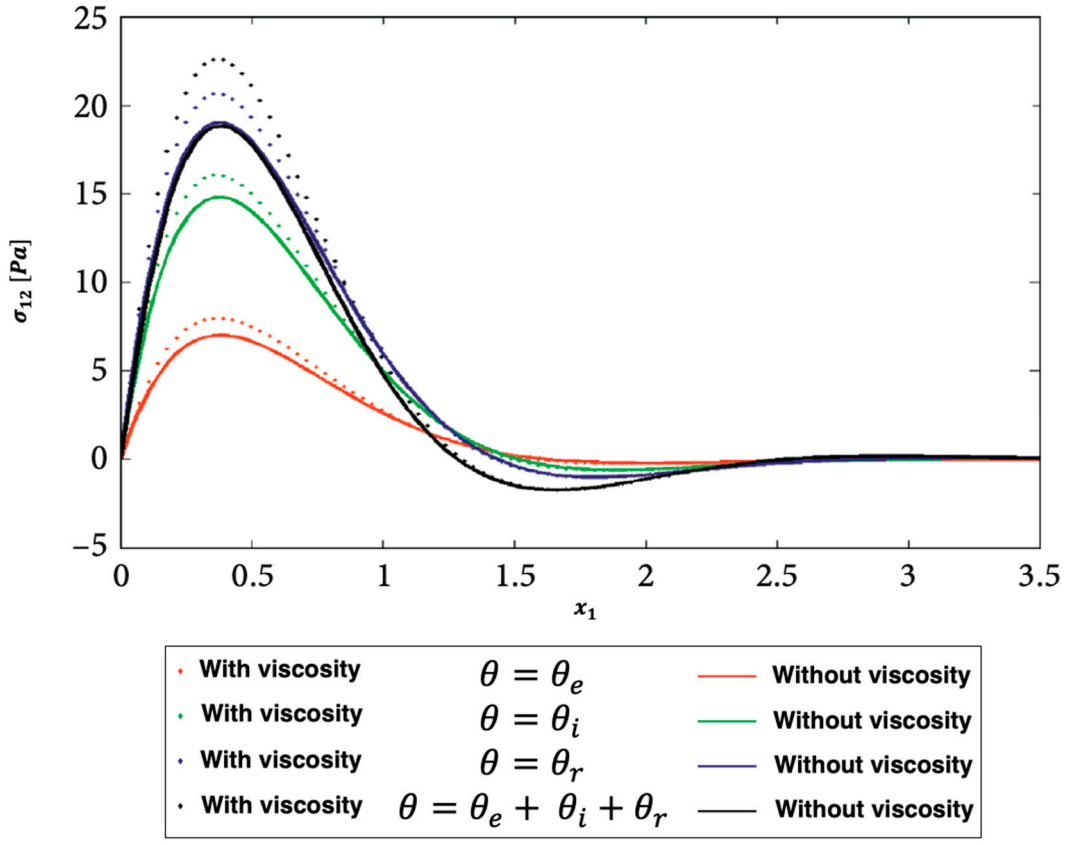

Figure 4. Propagation of the nonlinear thermal stress σ_{12} waves along x_1-axis for electron, ion, phonon and total 3T with and without viscosity effect.

Preprints (www.preprints.org) | NOT PEER-REVIEWED | Posted: 25 April 2023 doi:10.20944/preprints202304.0908.v1

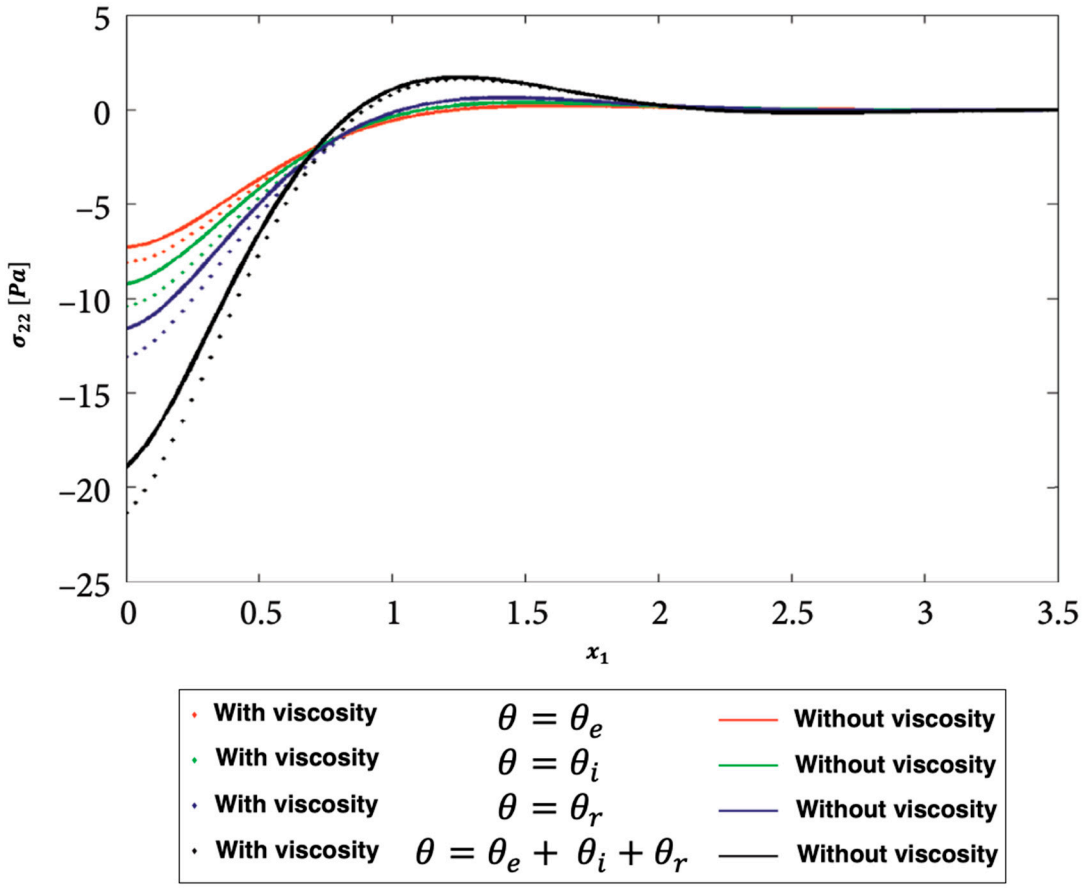

Figure 5. Propagation of the nonlinear thermal stress σ_{22} waves along x_1-axis for electron, ion, phonon and total 3T with and without viscosity effect.

Figures 6, 7 and 8 show the distributions of the nonlinear thermal stress σ_{11}, σ_{12}, and σ_{22} waves along x_1-axis for electron, ion, phonon and total 3T for isotropic and anisotropic viscoelastic porous structures. Figure 6 shows the distribution of the nonlinear thermal stress σ_{11} waves for electron ($\theta = \theta_e$), ion ($\theta = \theta_i$), phonon ($\theta = \theta_r$), and total ($\theta = \theta_e + \theta_i + \theta_r$) for isotropic and anisotropic viscoelastic porous structures. Figure 7 shows the distribution of the nonlinear thermal stress σ_{12} waves for electron ($\theta = \theta_e$), ion ($\theta = \theta_i$), phonon ($\theta = \theta_r$), and total ($\theta = \theta_e + \theta_i + \theta_r$) for isotropic and anisotropic viscoelastic porous structures. Figure 8 shows the distribution of the nonlinear thermal stress σ_{22} waves for electron ($\theta = \theta_e$), ion ($\theta = \theta_i$), phonon ($\theta = \theta_r$), and total ($\theta = \theta_e + \theta_i + \theta_r$) for isotropic and anisotropic viscoelastic porous structures.

Preprints (www.preprints.org) | NOT PEER-REVIEWED | Posted: 25 April 2023 doi:10.20944/preprints202304.0908.v1

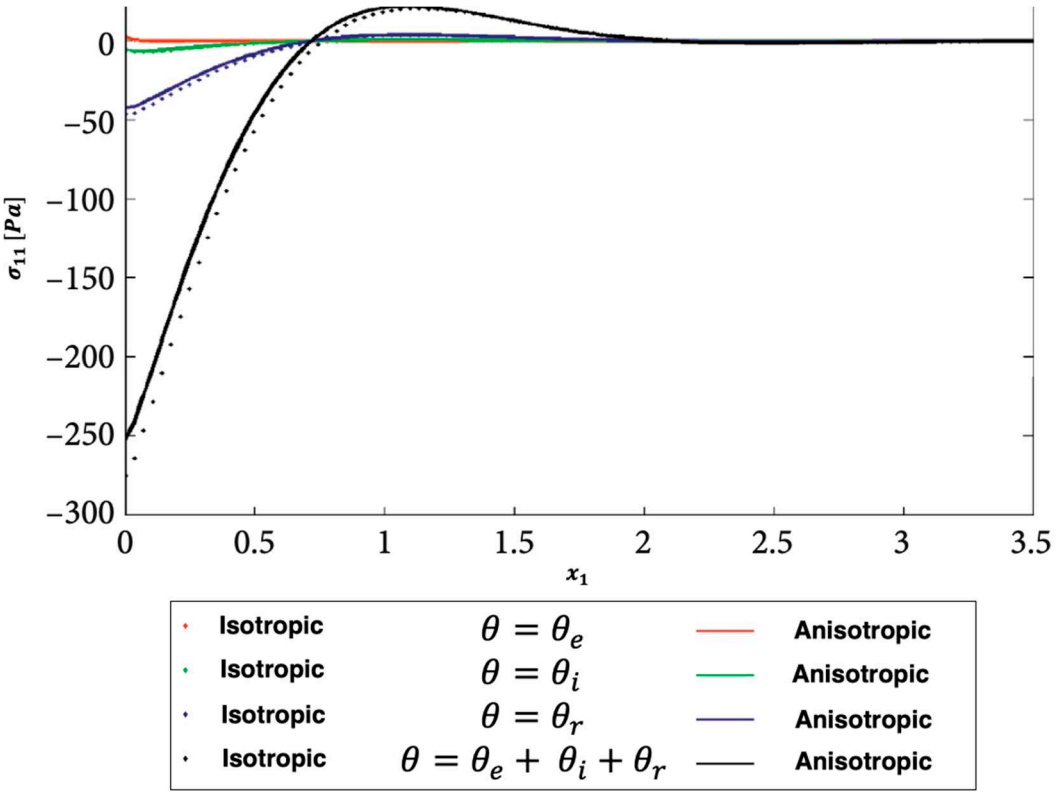

Figure 6. Propagation of the nonlinear thermal stress σ_{11} waves along x_1-axis for electron, ion, phonon and total 3T for isotropic and anisotropic viscoelastic porous structures.

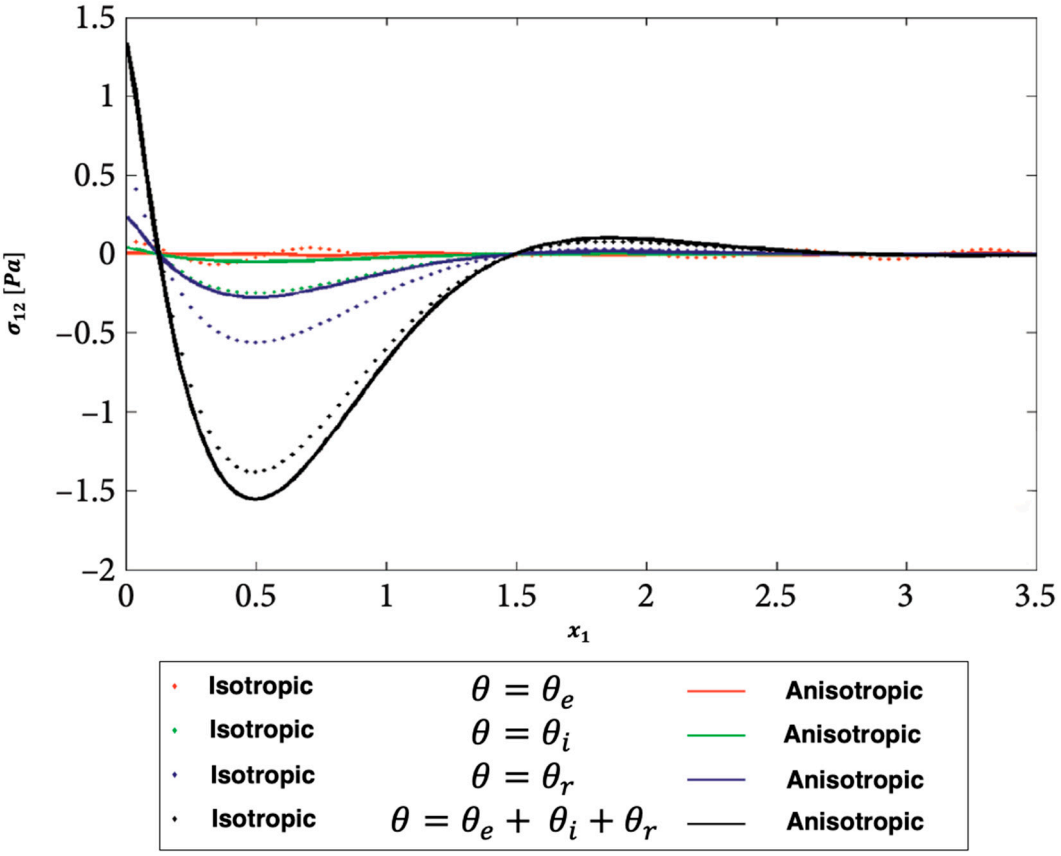

Figure 7. Propagation of the nonlinear thermal stress σ_{12} waves along x_1-axis for electron, ion, phonon and total 3T for isotropic and anisotropic viscoelastic porous structures.

Preprints (www.preprints.org) | NOT PEER-REVIEWED | Posted: 25 April 2023 doi:10.20944/preprints202304.0908.v1

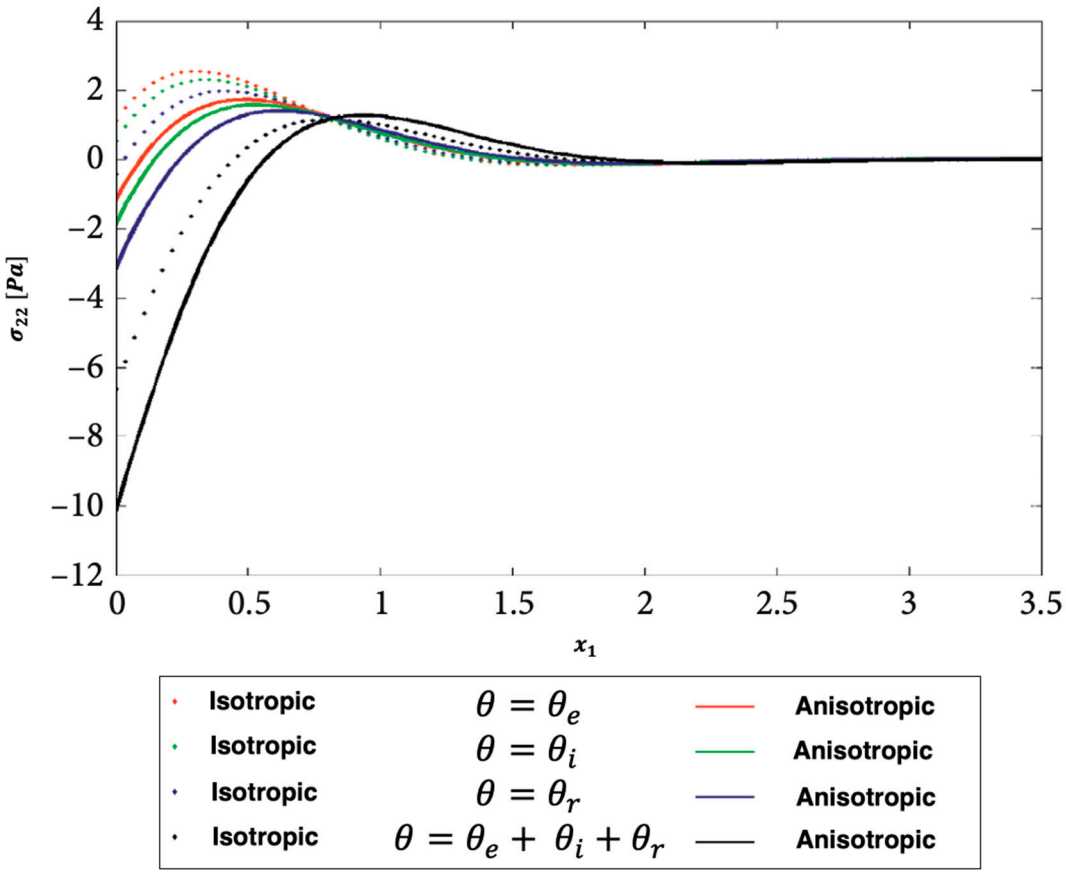

Figure 8. Propagation of the nonlinear thermal stress σ_{22} waves along x_1-axis for electron, ion, phonon and total 3T for isotropic and anisotropic viscoelastic porous structures.

The validity of the outcomes of the suggested technique was not supported by any published works. On the other hand, some literary works can be seen as special cases of the considered general work.

Figures 9, 10 and 11 show the distributions of the nonlinear thermal stress σ_{11}, σ_{12}, and σ_{22} waves along x_1-axis for electron, ion, phonon and total 3T using the finite difference method (FDM) [44] and current BEM. Figure 9 shows the distribution of the nonlinear thermal stress σ_{11} waves for electron ($\theta = \theta_e$), ion ($\theta = \theta_i$), phonon ($\theta = \theta_r$), and total ($\theta = \theta_e + \theta_i + \theta_r$) for FDM and BEM. Figure 10 shows the distribution of the nonlinear thermal stress σ_{12} waves for electron ($\theta = \theta_e$), ion ($\theta = \theta_i$), phonon ($\theta = \theta_r$), and total ($\theta = \theta_e + \theta_i + \theta_r$) for FDM and BEM. Figure 11 shows the distribution of the nonlinear thermal stress σ_{22} waves for electron ($\theta = \theta_e$), ion ($\theta = \theta_i$), phonon ($\theta = \theta_r$), and total ($\theta = \theta_e + \theta_i + \theta_r$) for FDM and BEM. These figures clearly show that the BEM and FDM are in excellent agreement, supporting the validity and precision of our proposed BEM approach.

Preprints (www.preprints.org) | NOT PEER-REVIEWED | Posted: 25 April 2023 doi:10.20944/preprints202304.0908.v1

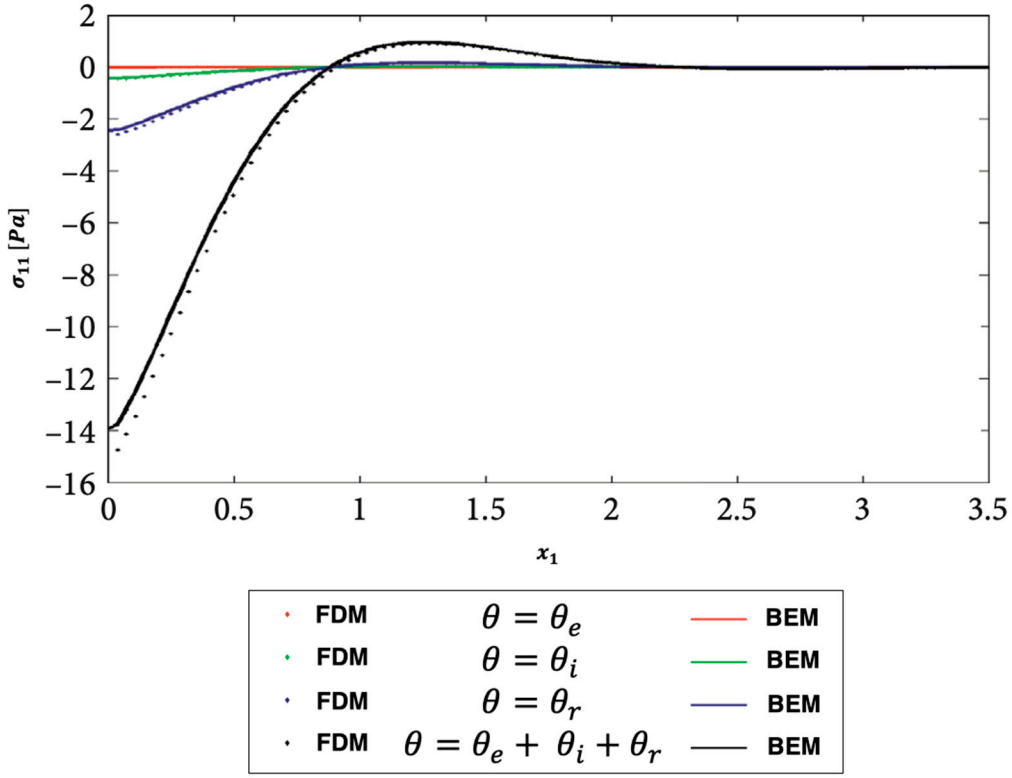

Figure 9. Propagation of the nonlinear thermal stress σ_{11} waves along x_1-axis for electron, ion, phonon and total 3T for FDM and BEM.

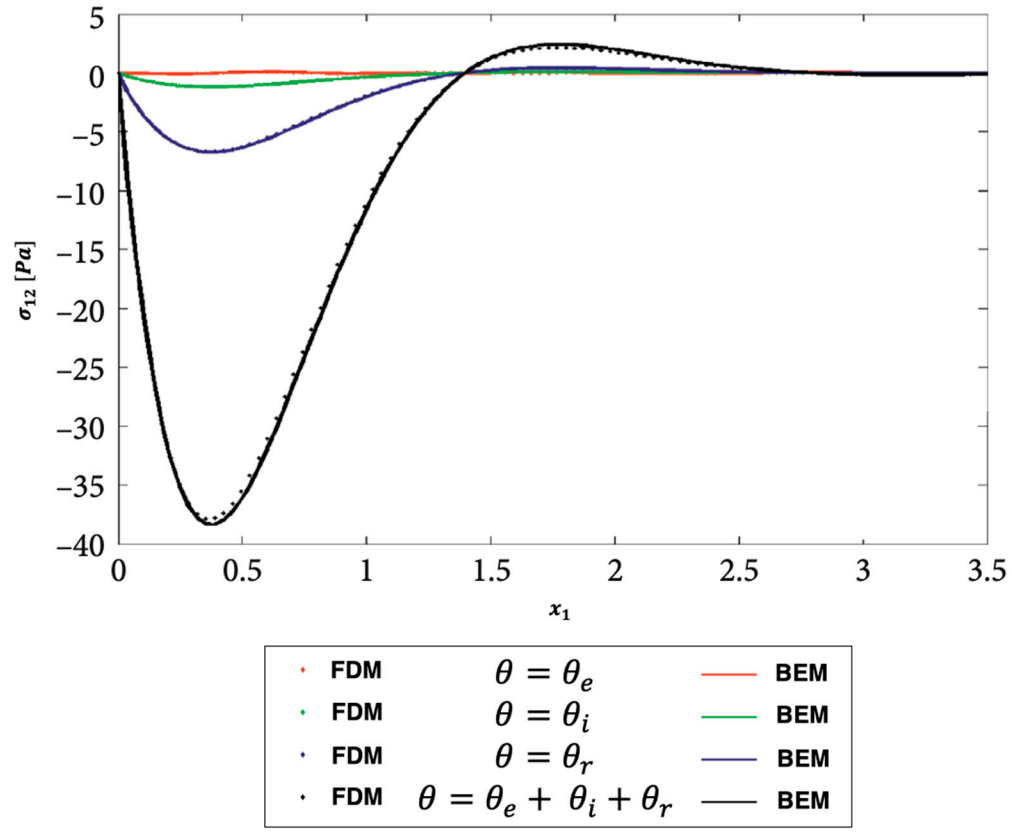

Figure 10. Propagation of the nonlinear thermal stress σ_{12} waves along x_1-axis for electron, ion, phonon and total 3T for FDM and BEM.

Preprints (www.preprints.org) | NOT PEER-REVIEWED | Posted: 25 April 2023 doi:10.20944/preprints202304.0908.v1

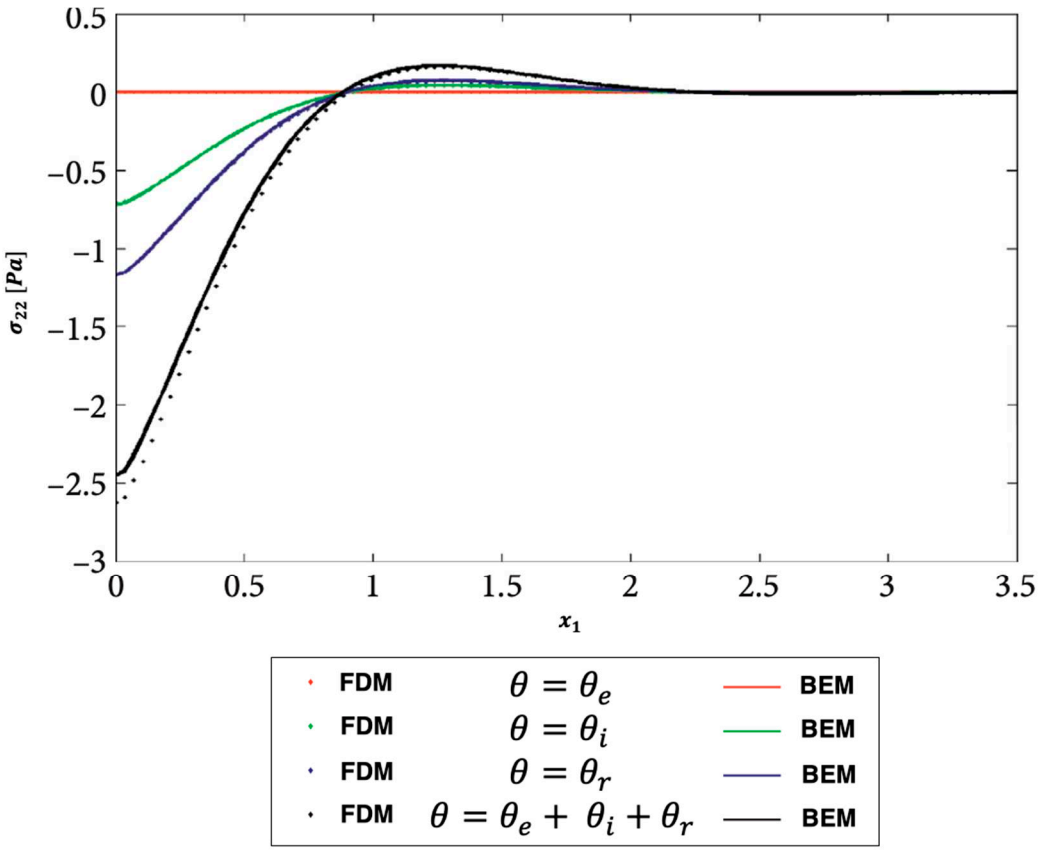

Figure 11. Propagation of the nonlinear thermal stress σ_{22} waves along x_1-axis for electron, ion, phonon and total 3T for FDM and BEM.

Table 1 shows a comparison of required computer resources for the current BEM results and FDM results of Hu et al. [44] of modeling of ultrasonic wave propagation problems in three-temperature anisotropic viscoelastic porous media.

Table 1. A comparison of the required computer resources for modeling of ultrasonic wave propagation problems in three-temperature anisotropic viscoelastic porous media.

	BEM	FDM
Number of nodes	66	40000
Number of elements	36	16000
CPU time (min)	2	160
Memory (MByte)	1	140
Disc space (MByte)	0	200
Accuracy of results (%)	1	2.0

6. Conclusion

The main goal of this article is to develop a novel boundary element model for describing ultrasonic thermomechanical interactions in three-temperature anisotropic viscoelastic porous media. Analytical or numerical solutions are always difficult due to the strong nonlinearity of ultrasonic wave propagation in three-temperature porous media problems, necessitating the development of new computational techniques. As a result, we employ a new BEM model to address such problems. The considered BEM model has low RAM and CPU usage due to its advantages such as dealing with more complex shapes of porous media and not requiring the discretization of the

Preprints (www.preprints.org) | NOT PEER-REVIEWED | Posted: 25 April 2023 doi:10.20944/preprints202304.0908.v1

internal domain. As a result, the considered BEM is a powerful and adaptable for modeling ultrasonic wave propagation in three-temperature anisotropic viscoelastic porous media. To obtain fundamental solutions, a double integral must be calculated, but this increases the total BEM computation time. To solve the current problem and improve formulation efficiency, we propose a BEM technique. The numerical results are graphed to show the effects of viscosity and anisotropy on nonlinear ultrasonic stress waves in porous media at three temperatures. The proposed methodology's validity, accuracy, and efficiency were demonstrated by comparing the obtained results to the corresponding solution obtained using the finite difference method (FDM). The findings of this paper contribute to the development of mathematical models that can be applied in biology, bioengineering and medicine

Funding: This research was funded by the Deanship of Scientific Research at Umm Al-Qura University, grant number 22UQU4340548DSR16. The APC was funded by the Deanship of Scientific Research at Umm Al-Qura University.

Data Availability Statement: All data generated or analyzed during this study are included in this published article.

Acknowledgments: The author would like to thank the Deanship of Scientific Research at Umm Al-Qura University for supporting this work, grant code 22UQU4340548DSR16.

Conflicts of Interest: The authors declare no conflict of interest.

Nomenclature

$*$	Convolution with respect to time	$\hat{g}_D$	Dirichlet datum
Γ	Boundary	$\hat{g}_N$	Neumann datum
Γ_D	Dirichlet boundary	J	Non-Gaussian temporal profile
Γ_N	Neumann boundary	J_0	Total energy intensity
δ_{ij}	Kronecker delta $(i,j=1,2)$	k_{ij}	Thermal conductivity tensor
ϵ	Linear strain tensor	$\mathbb{K}_\alpha$	Heat conductive coefficients
θ	Temperature field	k	poroelastic freedom degrees
μ_0	Shear moduli	n	Outward unit normal vector
χ	Viscoelastic constant	$\bar{p}$	Fluid pressure
ζ	Fluid volume variation	p_i	Singular points
ρ	$=\rho_e(1-\phi)+\phi\rho_f$ Bulk density	$\mathbf{q}$	Specific flux of the fluid
ρ_e	Elastic density	R	$=\lvert\mathbf{y}-\mathbf{x}\rvert$ Euclidean distance
ρ_f	Fluid density	Q	Heat source intensity
σ	Total stress tensor	R	Irradiated surface absorptivity
τ	Time	$\hat{\mathbf{t}}^g$	Generalized tractions
τ_1	Laser pulse time characteristic	Tr	Trace of a matrix
ϕ	$=\frac{V^f}{V}$ Porosity	$\widehat{\mathbf{U}}_r^s(\mathrm{r})$	Regular displacement
Ω	Region	$\widehat{\mathbf{U}}_s^s(\mathrm{r})$	Singular displacement
A	$=\phi(1+Q/R)$ Biot's coefficient	$\mathbf{u}$	Displacement
$\mathfrak{B}$	Stress-temperature coefficients	$\mathbf{u}_f$	Fluid displacement
$B_{\tilde{x}}^e$	Linear elastostatics operator	ν	Poisson's ratio
c	Specific heat	$\mathbb{W}_{ei}$ & $\mathbb{W}_{ep}$	Energy exchanging coefficients
C_{ajlg}	Constant elastic moduli	$\mathbb{W}_{ei}$	$=\rho\mathbb{A}_{ei}\theta_e^{-2/3}$
E_i	Young's moduli	$\mathbb{W}_{ep}$	$=\rho\mathbb{A}_{ep}\theta_e^{-1/2}$
$\mathbf{F}$	Body forces	x,y	Space coordinates
G_{ij}	Shear moduli	$\mathbf{x}$	Source point
		$\mathbf{y}$	Considered point

References

1. Nayak, M.K.; Dash, G.C.; Singhc, L.P. Steady MHD flow and heat transfer of a third grade fluid in wire coating analysis with temperature dependent viscosity. *Int. J. Heat Mass Transf.* **2014**, *79*, 1087–1095.
2. Nayak, M.K.; Dash, G.C.; Singh, L.P. Unsteady radiative MHD free convective flow and mass transfer of a viscoelastic fluid past an inclined porous plate. *Arab. J. Sci. Eng.* **2015**, *40*, 3029–3039.
3. Nayak, M.K. Chemical reaction effecton MHD viscoelastic fluid over a stretching sheet through porous medium. *Meccanica* **2016**, *51*, 1699–1711.
4. Fahmy, MA. Design Optimization for A Simulation of Rotating Anisotropic Viscoelastic Porous Structures Using Time-Domain OQBEM. *Math. Comput. Simul.* **2019**, *66*, 193–205.
5. Fahmy, M.A. Modeling and Optimization of Anisotropic Viscoelastic Porous Structures Using CQBEM and Moving Asymptotes Algorithm. A*rabian J. Sci. Eng.* **2019**, *44*, 1671–1684.
6. Fahmy, M.A.; Shaw, S.; Mondal, S.; Abouelregal, A.E.; Lotfy, K.; Kudinov, I.A.; Soliman, A.H. Boundary Element Modeling for Simulation and Optimization of Three-Temperature Anisotropic Micropolar Magneto-thermoviscoelastic Problems in Porous Smart Structures Using NURBS and Genetic Algorithm. *Int. J. Thermophys.* **2021**, *42*, 29.
7. Othman, M.I.A.; Fekry, M. Effect of Magnetic Field on Generalized Thermo-viscoelastic Diffusion Medium with Voids. *Int. J. Struct. Stab. Dyn.* **2016**, *16*, 1550033.
8. Othman, M.I.A.; Fekry, M.; Marin, M. Plane Waves in Generalized Magneto-thermo-viscoelastic Medium with Voids under the Effect of Initial Stress and Laser Pulse Heating. *Struct. Eng. Mech.* **2020**, *73*, 621–629.
9. Othman, M.I.A.; Fekry, M. Effect of Rotation and Gravity on Generalized Thermo-viscoelastic Medium with Voids. *Multi. Model. Mater. Struct.* **2018**, *14*, 322–338.
10. Othman, M.I.A.; Zidan, M.E.M.; Mohamed, I.E.A. Dual-phase-lag model on thermo-microstretch elastic solid under the effect of initial stress and temperature-dependent. *Steel Compos. Struct.* **2021**, *38*, 355–363.
11. Xu, Z.D.; Ge, T.; Liu, J. Experimental and theoretical study of high energy dissipation viscoelastic dampers based on acrylate rubber matrix. *ASCE J. Eng. Mech.* **2020**, *146*, 04020057.
12. Pei, R.Z.; Jing, L.; Cheng, W.C.; Xue, J.P. Boundary element method (BEM) for solving normal or inverse bio-heat transfer problem of biological bodies with complex shape. *J. Therm. Sci.* **1995**, *4*, 117–124.
13. Ooi, E.H.; Ang, W.T.; Ng, E.Y.K. A boundary element model for investigating the effects of eye tumor on the temperature distribution inside the human eye. *Comput. Biol. Med.* 2009, 39, 667-677.
14. Zhou, J.; Chen, J.K.; Zhang, Y. Simulation of Laser-Induced Thermotherapy Using a Dual-Reciprocity Boundary Element Model with Dynamic Tissue Properties. *IEEE Trans. Biomed. Eng.* **2010**, *57*, 238–245.
15. Ng, E.Y.K.; Tan, H.M.; Ooi, E.H. Boundary element method with bioheat equation for skin burn injury. *Burns* **2009**, *35*, 987–997.
16. Majchrzak, E.; Turchan, L. The general boundary element method for 3D dual-phase lag model of bioheat transfer. *Eng. Anal. Bound. Elem.* **2015**, *50*, 76–82.
17. Bottauscio, O.; Chiampi, M.; Zilberti, L. Boundary Element Solution of Electromagnetic and Bioheat Equations for the Simulation of SAR and Temperature Increase in Biological Tissues. *IEEE Trans. Magn.* **2012**, *48*, 691–694.
18. Deng, Z.S.; Liu, J. Modeling of multidimensional freezing problem during cryosurgery by the dual reciprocity boundary element method. *Eng. Anal. Bound. Elem.* **2004**, *28*, 97–108.
19. Partridge, P.W.; Wrobel, L.C. A coupled dual reciprocity BEM/genetic algorithm for identification of blood perfusion parameters. *Int. J. Numer. Methods Heat Fluid Flow* **2009**, *19*, 25–38.
20. Chan, C.L. Boundary Element Method Analysis for the Bioheat Transfer Equation. *J. Biomech. Eng.* 1992, 114, 358-365.
21. Wrobel, L.C. *The Boundary Element Method, Applications in Thermos-Fluids and Acoustics*; Wiley: New York, NY, USA, 2002; Volume 1.
22. Lua, W.Q.; Liub, J.; Zenga, Y. Simulation of the thermal wave propagation in biological tissues by the dual reciprocity boundary element method. *Eng. Anal. Bound. Elem.* **1998**, *22*, 167–174.
23. Fahmy, M.A. A time-stepping DRBEM for magneto-thermo-viscoelastic interactions in a rotating nonhomogeneous anisotropic solid. *Int. J. Appl. Mech.* **2011**, *3*, 711–734.
24. Fahmy, M.A. A time-stepping DRBEM for the transient magneto-thermo-visco-elastic stresses in a rotating non-homogeneous anisotropic solid. *Eng. Anal. Bound. Elem.* **2012**, *36*, 335–345.
25. Fahmy, M.A. Transient magneto-thermoviscoelastic plane waves in a non-homogeneous anisotropic thick strip subjected to a moving heat source. *Appl. Math. Modell.* **2012**, *36*, 4565–4578.

26. Fahmy, M.A. The effect of rotation and inhomogeneity on the transient magneto-thermoviscoelastic stresses in an anisotropic solid. *ASME J. Appl. Mech.* **2012**, *79*, 051015.
27. Fahmy, M.A. Implicit-Explicit time integration DRBEM for generalized magneto-thermoelasticity problems of rotating anisotropic viscoelastic functionally graded solids. *Eng. Anal. Bound. Elem.* **2013**, *37*, 107–115.
28. Fahmy, M.A. Generalized magneto-thermo-viscoelastic problems of rotating functionally graded anisotropic plates by the dual reciprocity boundary element method. *J. Therm. Stress.* **2013**, *36*, 1–20.
29. Fahmy, M.A. Shape design sensitivity and optimization for two-temperature generalized magneto-thermoelastic problems using time-domain DRBEM. *J. Therm. Stress.* **2018**, *41*, 119–138.
30. Fahmy, M.A. Shape design sensitivity and optimization of anisotropic functionally graded smart structures using bicubic B-splines DRBEM. *Eng. Anal. Bound. Elem.* **2018**, *87*, 27–35.
31. Fahmy, M.A. Boundary Element Algorithm for Modeling and Simulation of Dual Phase Lag Bioheat Transfer and Biomechanics of Anisotropic Soft Tissues. *Int. J. Appl. Mech.* **2018**, *10*, 1850108.
32. Hosseini, M.; Paparisabet, M.A. The Effects of Blood Flow on Blood Vessel Buckling Embedded in Surrounding Soft Tissues. *Int. J. Appl. Mech.* **2016**, *8*, 1650065.
33. Azzez, K.; Chaabane, M.; Abellan, M.A.; Bergheau, J.M.; Zahouani, H.; Dogui, A. Relevance of Indentation Test to Characterize Soft Biological Tissue: Application to Human Skin. *Int. J. Appl. Mech.* **2018**, *10*, 1850074.
34. Biot, M.A. Theory of propagation of elastic waves in a fluid- saturated porous solid. II. Higher frequency range. *J. Acoust. Soc. Am.* **1956**, *28*, 179–191.
35. Schanz, M. *Wave Propagation in Viscoelastic and Poroelastic Continua*; Lecture Notes in Applied Mechanics; Springer: New York, NY, USA, 2001; Volume 2.
36. Bonnet, G. Basic singular solutions for a poroelastic medium in the dynamic range. *J. Acoust. Soc. Am.* **1987**, *82*, 1758–1763.
37. Messner, M.; Schanz, M. A regularized collocation boundary element method for linear poroelasticity. *Comput. Mech.* **2011**, *47*, 669–680.
38. Ding, C. A Symmetric Successive Overrelaxation (SSOR) based Gauss- Seidel Massive MIMO Detection Algorithm. *J. Phys. : Conf. Ser.* **2020**, *1438*, 012005.
39. Steinbach, O. *Numerical Approximation Methods for Elliptic Boundary Value Problems*; Springer: New York, NY, USA, 2008.
40. Kielhorn, L. A time-domain symmetric Galerkin BEM for viscoelastodynamics. In *Computation in Engineering and Science*; Brenn, G., Holzapfel, G.A., Schanz, M., Steinbach, O., Eds.; Graz University of Technology, Institute of Applied Mechanics: Austria, 2009.
41. Lubich, C. Convolution quadrature and discretized operational calculus. I. *Numer. Math.* **1988**, *52*, 129–145.
42. Lubich, C. Convolution quadrature and discretized operational calculus II. *Numer. Math.* **1988**, *52*, 413–425.
43. Morrow, D.A.; Haut Donahue, T.L.; Odegard, G.M.; Kaufman, K.R. Transversely isotropic tensile material properties of skeletal muscle tissue. *J. Mech. Behav. Biomed. Mater.* **2010**, *3*, 124–129.
44. Hu, N.; Wang, M.; Qiu, B.; Tao, Y. Numerical Simulation of Elastic Wave Field in Viscoelastic Two-Phasic Porous Materials Based on Constant Q Fractional-Order BISQ Model. *Materials* **2022**, *15*, 1020. https://doi.org/10.3390/ma15031020.